Depth-resolved magnetic structure across the ferromagnetic to helical-antiferromagnetic phase transition in Dy/W(110)

H. Ott,[1,*] C. Schüßler-Langeheine,[1,2,3] E. Schierle,[1,3] E. Weschke,[1,3] and G. Kaindl[1]
[1]*Institut für Experimentalphysik, Freie Universität Berlin, 14195 Berlin, Germany*
[2]*II. Physikalisches Institut, Universität zu Köln, Zülpicher Str. 77, 50937 Köln, Germany*
[3]*Helmholtz-Zentrum Berlin für Materialien und Energie GmbH, Albert-Einstein-Str. 15, 12489 Berlin, Germany*
(Received 19 June 2010; published 3 December 2010)

We investigated the magnetic depth profile during the transition from the ferromagnetic (FM) to the helical-antiferromagnetic (AFM) phase in Dy-metal films grown on W(110). To this purpose, we used the strongly varying photon penetration depth across the Dy M_5 absorption threshold in resonant magnetic soft x-ray diffraction. Unlike in earlier studies on Dy films with two equivalent interfaces, we find a gradual growth of the AFM part of the film with temperature. The near-surface magnetic structure does not become FM and appears to serve as seed layer for the growth of the AFM order.

DOI: 10.1103/PhysRevB.82.214408 PACS number(s): 75.70.−i, 61.05.cf, 75.25.−j

I. INTRODUCTION

Near surfaces and interfaces, magnetic properties usually deviate clearly from those of the respective bulk material. Knowledge about changes in magnetic properties near boundaries is of utmost importance for technical applications involving magnetic layers. Also, if surface sensitive experimental methods—such as tunneling spectroscopy or photoelectron spectroscopy—are used, one should be aware that the changed surface properties can strongly influence the results due to the finite probing depth.

Many interesting magnetic materials can be found among rare-earth (RE) systems. The elemental RE metals are considered prototypes of local-moment magnets. Their strong magnetic moments that are essentially carried by the partially filled 4*f* shell are coupled via indirect exchange interaction that—together with strong anisotropies—leads to a large variety of magnetic structures including helical and conical structures as well as those with spatially modulated moments. With temperature, several of the RE metals undergo a antiferromagnetic (AFM) to either ferromagnetic (FM) (Tb, Dy) or ferrimagnetic (Ho) phasetransition.

The coupling between magnetic and electronic structures in RE systems has been subject of various theoretical and experimental studies. One topic of interest is the influence of magnetic order on band structure. Since the 4*f* moments are local and largely temperature independent on the temperature scale of the respective ordering temperatures, a local interaction between 4*f* and more localized valence states should lead to an energy splitting in the band structure even in the paramagnetic phase.[1,2] Such a behavior was indeed experimentally observed by scanning tunneling microscopy for the surface states on various (0001) surfaces of RE metals[3–6] and by photoelectron spectroscopy for a surface-oxide phase.[7,8] A related question is to what extent more delocalized states monitor a spatial average of the 4*f* magnetic moment. However, surface sensitive photon-electron-spectroscopy experiments on FM Gd and helical-AFM Tb, Dy, and Ho did not indicate an influence of the kind of long-range magnetic order on the exchange splitting of delocalized bands.[9–11]

Many of the experiments in this field were carried out on *in situ* grown epitaxial films, mostly on W or Mo, which are easier to prepare with high purity and surface quality than bulk single crystals. Fortunately, these films show essentially bulklike magnetic structures as has been confirmed, e.g., by magnetic x-ray scattering from helical-AFM Ho thin films.[12,13] Noticeable deviations from bulk behavior where shown to occur only for thicknesses below 20 monolayers (MLs). While such bulklike structure apply for the larger part of the film, deviations near the surface and interface occur, but are not easy to observe. An important question for the interpretation of experimental results for RE metal films is, e.g., in which part of the film and to what extent strain affects the magnetic phase transitions that couples via magnetoelastic effects to the lattice.

Elementary Dy exhibits both a FM and an AFM phase separated by a first-order phase transition.[14] Between the Néel temperature of T_N=179 K and the Curie temperature of T_C=89 K, bulk Dy metal is a helical AFM, characterized by a ferromagnetic alignment of the 4*f* moments within the basal plane of the hcp lattice; the magnetic moments of neighboring planes are rotated by a certain angle ϕ_H (see Fig. 1), thus forming a helical structure along the crystallographic *c* axis. The transition from the helical phase to the FM low-temperature phase is a hysteretic first-order transition: it is characterized by a discontinuity of all lattice parameters due to a orthorhombic distortion in the FM phase.[15] In thin films and multilayers, this phase transition can be strongly influenced by the film boundaries: the influence of strain on this phase transition has been studied in detail for Dy-metal films embedded between layers of Y_xLu_{1-x};[16] by choice of the Y/Lu ratio, either compressive or expansive strain can be applied to the Dy film and by that T_C can be reduced or increased smoothly over a wide temperature range while conserving the discontinuous first-order character of the phase transition.[16]

Up to now, the influence of strain on thin films of Dy metal has only been studied in systems with two identical boundary layers.[16–18] Here, we report on the phase transition in samples with inequivalent boundaries, which turns out to behave distinctly different from the symmetric systems studied so far. We shall show in the following by magnetic depth

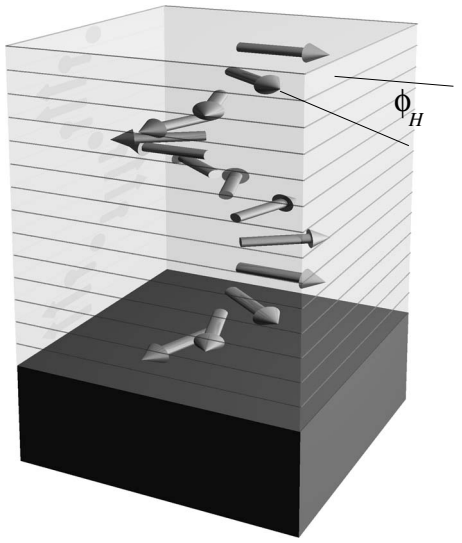

FIG. 1. Illustration of the helical-AFM structure of Dy metal. The arrows represent the magnetization direction of the corresponding single atomic layer. The direction of magnetization is rotated by an angle ϕ_H with respect to the neighboring layer leading to the helical magnetic structure.

profiling using resonant soft x-ray diffraction[19] that near the Dy/W interface the FM-to-AFM phase transition is substantially shifted to higher temperatures leading to a gradual development of the helical phase over a wide temperature range. Furthermore, we show that the magnetic structure near the Dy surface does not become FM but instead serve as seed layer for the AFM order.

II. EXPERIMENTAL

The scattering experiments were performed using two different experimental setups suited for two different photon-energy regions. The combined studies of the crystalline and magnetic structure were carried out at the ID10A undulator beamline of the European Synchrotron Radiation Facility (ESRF) in Grenoble, France, using 7780 eV x rays selected by a diamond(111) monochromator crystal in Laue geometry. The Dy-metal films were epitaxially grown *in situ* in a small ultrahigh-vacuum (UHV) chamber, which is equipped with Be windows for the incoming and outgoing beam. This UHV chamber can be directly attached to the diffractometer. In order to discriminate the magnetic scattering from the charge scattering contribution, polarization analysis was applied to the scattered beam using a graphite crystal on a two-circle analyzer stage.[20]

The soft x-ray scattering experiments were performed at the U49/1-SGM, UE52-SGM, and U49/2-PGM1 beamlines at BESSY II in Berlin. We used a home-built two-circle diffractometer insight an UHV chamber that was directly attached to the beamline. A silicon diode behind an adjustable slit served as photon detector. The scattering geometry was horizontal in both cases, with linear polarization of the incident beam in horizontal direction.

In both setups the Dy-metal films were grown *in situ*. The chambers are equipped with a set of e-beam evaporators, a commercial quartz balance for thickness control, and a mass spectrometer for residual gas analysis. The samples were cooled by a closed-cycle He refrigerator. For all experiments, the same W(110) substrate and the same evaporators were used. 99.99% pure metal was evaporated from a Ta crucible heated by electron bombardment. The residual gas pressure was below 10^{-10} mbar. The films were grown in two steps with the substrate held at room temperature. After growth of a 20-ML-thick seed layer, the sample was annealed to 680 K, and after reaching the final thickness, the sample was annealed to 880 K. This procedure leads to well-ordered clean films as checked by x-ray reflectivity measurements, x-ray diffraction, and photoelectron spectroscopy.

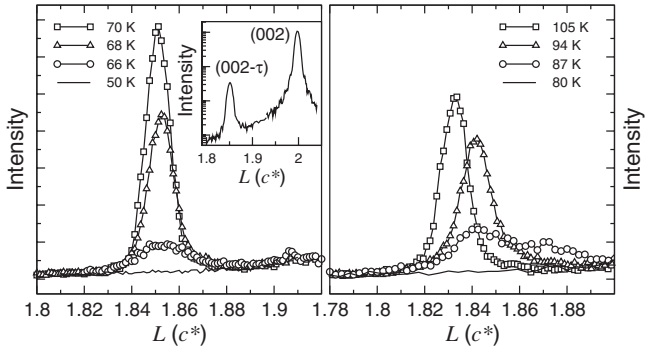

FIG. 2. Temperature-dependent reflectivity scans of the $(002-\tau)$ magnetic satellite measured from a 184-ML-thick Dy film on W(110) across the FM-to-helical-AFM phase transition. Left: spectra recorded at various temperatures during cooling down. Right: spectra recorded on warming up. The inset displays the Dy(002) Bragg peak and the $(002-\tau)$ superstructure satellite at 70 K on cooling down.

III. CONVENTIONAL X-RAY SCATTERING

In order to characterize the crystalline and magnetic structure of the Dy films grown on W(110) as well as the transition between the FM and the helical-AFM phase, experiments in the conventional x-ray regime at 7780 eV (Dy L_3 resonance) were carried out. In this energy region absorption effects are small and all film layers contribute to the scattered signal with almost the same magnitude. At this photon energy both the crystalline and the magnetic structure can be studied: the helical superstructure leads to additional reflections that occur at $(002n \pm \tau)$ in units of the Dy reciprocal lattice parameter c^* with $n=0,1,2,\ldots$ and $\tau=2\times\phi_H/360°$ (see inset of Fig. 2). Due to the beryllium windows of the UHV chamber, the scattering angle 2Θ was limited to 20°, which is sufficient to reach the (002) Bragg peak and the $(002\pm\tau)$ magnetic satellites. Magnetic diffraction data from a 180-ML-thick Dy film on W(110) are shown in Fig. 2; the scans were taken along the [001] (L) direction. The left panel displays spectra recorded upon cooling through the phase transition from the AFM to the FM phase. The phase transition leads to a decreasing satellite intensity due to the disappearance of AFM order. The right panel shows the spectra recorded upon heating from the FM to the AFM phase. While upon cooling, the satellite is most intense at 70 K, it

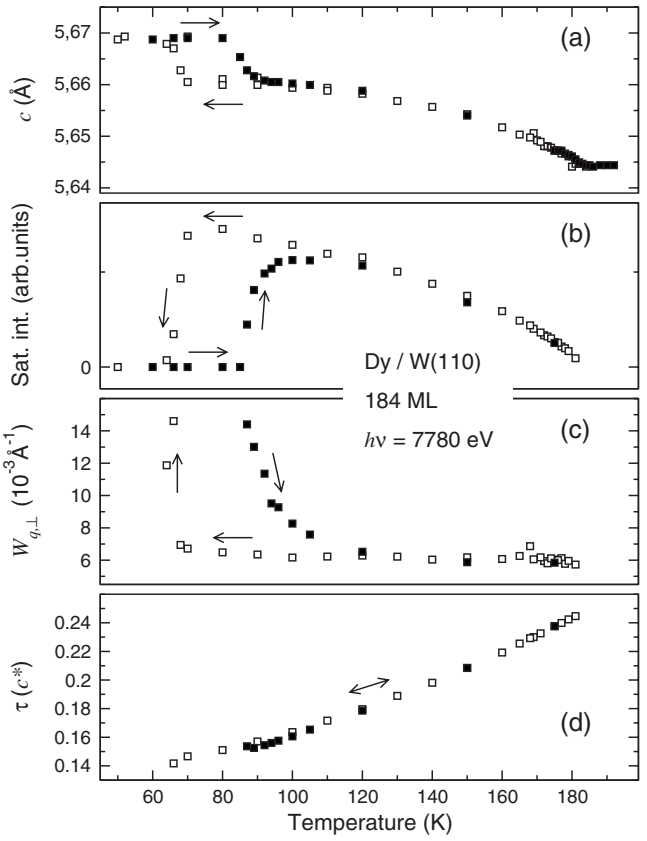

FIG. 3. From top: (a) c-axis lattice parameter, (b) integrated intensity of the $(002-\tau)$ magnetic satellite, (c) longitudinal width [half width at half maximum (HWHM)] $W_{q,\perp}$ of the magnetic satellite, and (d) magnetic modulation vector τ as a function of temperature. Open symbols: cooling down from well above the highest ordering temperature and filled symbols: measured on the warming-up path.

has not even reappeared when the sample is heated to 80 K; this clearly shows the hysteretic character of the phase transition.

Information on the magnetic structure can be obtained from the intensity, width, and position of the magnetic satellite and—because of magnetoelastic coupling—also from the position of the structural Bragg peaks. The results of the analysis are summarized in Fig. 3. First, we concentrate on the two upper curves, (a) the c-axis lattice parameter as obtained from the (002) Bragg peak position and (b) the integrated intensity of the $(002-\tau)$ magnetic satellite: as expected for a first-order phase transition, the data reveal a pronounced hysteresis for both quantities. Around 68 K, the c-axis parameter shows the characteristic expansion upon cooling (open symbols) into the FM phase while the intensity of the magnetic-superstructure satellite drops in the same temperature interval. Upon heating (filled symbols), the c-axis parameter relaxes to its lower value with a hysteresis of about 20 K. With the same hysteresis, the magnetic satellite intensity starts to grow upon heating, which indicates the reappearance of the helical-AFM phase; however, the magnetic satellite intensity does not jump back to the value it exhibited on cooling down. While during the transition from the helical-AFM to the FM phase at about 68 K the satellite intensity vanishes within a temperature interval of about 5 K, the helical structure develops on the way back much more gradual. Only about 35 K above its appearance temperature, the helical structure has fully recovered. Such a behavior has not been reported so far for bulk Dy and not for Dy films with equal boundaries.

The behavior of the longitudinal width, $W_{q,\perp}$, of the magnetic satellite, displayed in Fig. 3(c), further characterizes this delayed transition: on the cooling path, $W_{q,\perp}$ has a constant value corresponding to the inverse film thickness; this reflects AFM order throughout the whole film. During the phase transition, the satellite broadens in the same temperature interval in which its intensity drops and eventually disappears. Upon heating, the satellite reappears with nearly the same width that it had right before it disappeared. Toward higher temperatures, the width decreases slowly, and it does not reach the value it had on the cooling path below that temperature, where also the satellite intensity has fully recovered. Since $W_{q,\perp}$ is inversely proportional to the number of atomic planes contributing to the helical structure, its slow decrease upon heating is the signature of a gradual growth of one or several helically ordered regions along the surface normal. Whether these regions grow laterally as well cannot be answered from this experiment because of the insufficient experimental resolution, which does not allow a statement about the magnetic in-plane coherence or the in-plane extension of the helical regions. In any case, it is obvious from the data that the FM phase is more stable in one part of the film than in the other. Considering the two inequivalent film boundaries, it is plausible to assume that one of them (or both, possibly with different strengths) stabilizes the FM order.

A particularly suspicious candidate to stabilize the FM order is the W/Dy interface, because the W(110) surface exhibits a very similar symmetry as the Dy basal plane in the FM phase, in which orthorhombic distortion breaks the hexagonal in-plane symmetry. From the data presented so far, however, this assumption can neither be proved nor can we determine in which way the helix grows. This is due to the fact that the probing depth for conventional x rays is larger than the film thickness and the information is hence averaged over the whole film. In Sec. IV we shall show that the tunable probing depth of soft x rays allows a detailed and conclusive analysis. Before we do that, we will have a look on the thickness dependence.

Like other boundary-related effects, the delay in the development of the magnetic structure is stronger in thinner films due to the increasing relative weight of the surface and interface. This tendency is reflected in the thickness dependence of the hysteresis as observed in the temperature dependence of the c-axis lattice parameter, which is displayed in Fig. 4. In bulk Dy (shown in the upper part of Fig. 4), the hysteresis is only about 5 K and the phase transition causes a sharp jump between the lower and the upper c-axis parameters, which characterize the helical-AFM and the FM phases, respectively. The reduction in the sample thickness leads to a softening of the hysteresis and a stronger delay in the appearance of the other magnetic phase. For a 47 ML film (lowest curve in Fig. 4), the hysteresis of the c-axis lattice parameter is hardly detectable at all; this reveals that

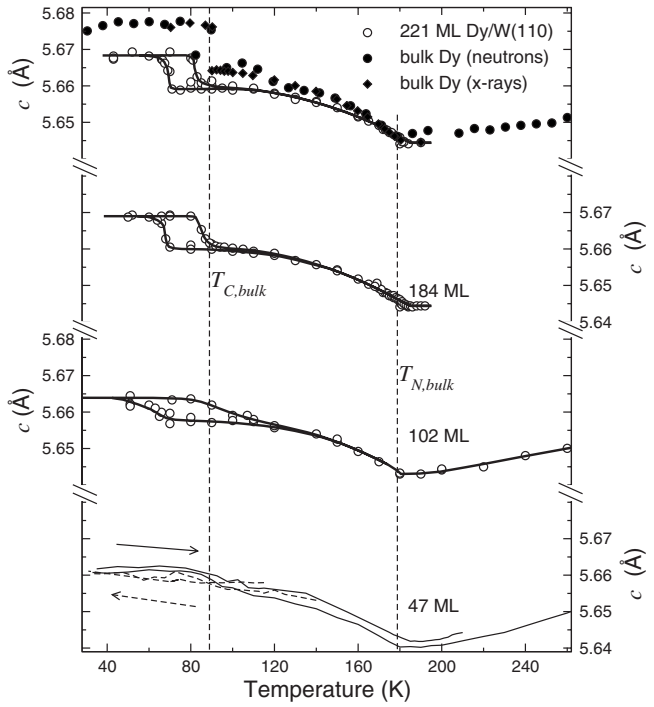

FIG. 4. *c*-axis lattice parameter of Dy films of different thicknesses grown on W(110). The data were obtained from the temperature dependence of the (002) Bragg-peak position. The upper panel shows additional bulk data measured from neutron scattering by Darnell *et al.* (Ref. 15) (filled circles) and from x-ray scattering by Helgesen *et al.* (Ref. 21) (filled diamonds).

the magnetic structure is fully dominated by surface and interface effects.

IV. MAGNETIC DEPTH PROFILES

A. Dimensionality

While a growth of the AFM order along the crystallographic *c* direction can be concluded from the data taken in the conventional x-ray region, the observation of lateral growth is limited by the moderate momentum resolution we could achieve in this energy range. This is a consequence of the rather weak diffraction intensity from a thin film even at the brightest synchrotron radiation source, which requires to open the detector slits leading to a worsening of the momentum resolution. Thus, an important open question so far is, whether the AFM regions grow laterally as well. This can be answered by our experiments in the soft x-ray region where the peak in momentum space is spread over a large angular interval, which allows us to easily reach a momentum resolution of 4×10^{-4} Å^{-1}. Figure 5 displays the results for the longitudinal width, $W_{q,\perp}$, and the width of the transverse scans, $W_{q,\parallel}$, measured at L_3 and near the M_5 resonance at 1305 eV. For $W_{q,\perp}$, essentially the same behavior is found in both photon-energy regions. The small deviation of the data obtained in the soft x-ray region from that recorded in the conventional hard x-ray regime can be attributed to a reduced photon penetration depth, as will be discussed further below. From the in-plane width, $W_{q,\parallel}$, no significant change

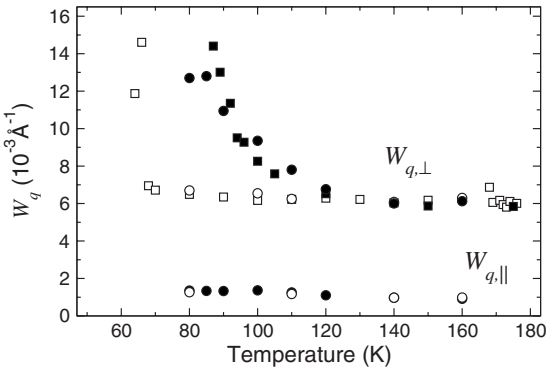

FIG. 5. Width (HWHM) of the $(002-\tau)$ magnetic satellite measured in the conventional x-ray region at 7780 eV (squares) and of the $(000+\tau)$ magnetic satellite measured at 1305 eV (circles), along the crystallographic *c* axis, $W_{q,\perp}$, and within the basal plane, $W_{q,\parallel}$. The data were recorded on the cooling path (open symbols) and on the warming path (filled symbols) as indicated by the arrows.

in the in-plane magnetic coherence length of about 1000 Å can be observed, neither for different temperatures nor between the cooling and the heating paths. This means that the growth of helically ordered sample regions can be considered to be a quasi-one-dimensional process along the direction of the crystallographic *c* axis only while it is laterally homogeneous at all temperatures. Note that the soft x-ray data were recorded with a photon energy, where the probing depth is comparable to the film thickness; the obtained in-plane coherence is hence representative for the whole AFM-ordered parts of the film.

B. Optical parameters across the M_5 resonance

To investigate a magnetic structure in a depth-resolved way, we make use of the dramatic change in the photon penetration depth across a strong resonance in the soft x-ray regime. A quantitative analysis of the scattering data and the probing depth requires the knowledge of the optical parameters while tabulated parameters are available off resonance,[22,23] these tables are not accurate enough at resonances, where the optical parameters vary strongly with photon energy. We obtained the optical parameters from specular-reflectivity curves taken from a 180-ML-thick Dy film in a state, where the helical magnetic structure is fully developed. The left panel of Fig. 6 shows reflectivity curves in the region of the $(000+\tau)$ magnetic satellite: far away from resonance, at 900 eV, the spectrum is dominated by charge scattering, and it shows the so-called Kiessig fringes arising from the interference between x rays reflected from the films surface and its interface with the W substrate. The magnetic-superstructure peak is very weak and only visible as a less pronounced minimum at $q_\perp \approx 0.185$ Å^{-1} on a logarithmic scale. Near the resonance at 1301 eV photon energy (middle spectrum), the magnetic signal is enhanced and a well pronounced magnetic satellite can be seen. The Kiessig fringes are damped because the penetration depth of the photons is now comparable to the film thickness and less signal comes from the interface. In case of the 1294 eV spectrum (top) the photon absorption is strong. The spectrum shows no

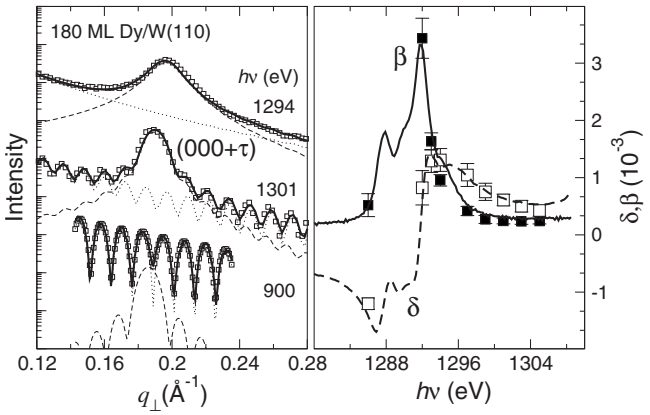

FIG. 6. Left: specular-reflectivity curves from a 180-ML-thick Dy film at various photon energies. The solid lines through the data points and the subspectra show the results of least-squares fit analysis. Dotted lines: charge scattering contribution. Dashed lines: contribution from the magnetic satellite. Right: optical parameters δ (open squares) and β (filled squares) as obtained from the fit analyses. The solid line represents β derived from the scaled experimental XAS with the corresponding Kramers-Kronig transform given by the dashed curve.

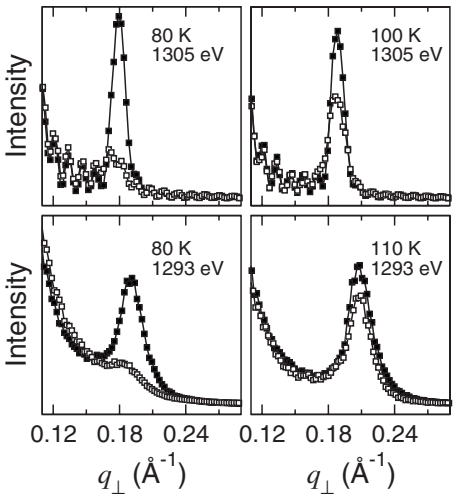

FIG. 7. Reflectivity curves from a 180-ML-thick Dy film recorded at 1305 eV (upper panels) and 1293 eV photon energy (lower panels) at two different temperatures (left and right panels). In each panel the data obtained on the cooling path (filled squares) are compared to the data measured at the same temperature but during warmup (open squares).

Kiessig fringes because there are no photons reflected from the interface, which also means that only a part of the sample volume is probed.

For a quantitative analysis, we fitted a realistic model to the data. The Kiessig fringes were described in the framework of a dynamical theory of reflectivity following Parratt;[24] they provide information on film thickness and roughness of surface and interface. The magnetic contribution to the data is described by the structure factor of the magnetic helix[25]

$$F(q_\perp) \propto P \cdot e^{-1/2q_\perp^2\sigma^2} \cdot \sum_{n=1}^{N} e^{ind(q_\perp-\tau)}, \qquad (1)$$

where P is a polarization factor, the Debye-Waller-type damping factor describes the effect of the roughness σ, N is the number of layers that contribute to the helix, and $d=c/2$ denotes the layer spacing along the c direction and corresponds to the magnetic modulation vector. Unlike in most conventional x-ray scattering experiments, the absorption and dispersion corrections cannot be neglected across a strong resonance; they are accounted for by a complex wave vector $q_\perp = 4\pi/\lambda \sin(\sqrt{\Theta^2 - 2\delta + i2\beta})$, with Θ being the incidence and detection angle measured with respect to the samples surface, and $n=1-\delta+i\beta$ the complex index of refraction.

Superpositions of the reflectivity and the magnetic signal describe all spectra taken at various photon energies in detail (solid lines), and the optical parameters, δ and β, can be obtained from the fits directly without adjustable parameters. The resulting values are shown on the right panel of Fig. 6: the solid line through the β values represents the measured M_5 x-ray absorption spectrum (XAS) as obtained by the sample drain current, scaled to the maximum β value (this is directly possible in a small energy interval). As a check of consistency, we find that the Kramers-Kronig transformation of the scaled XAS (dashed line) reproduces the δ values obtained from the reflectivity curves. As expected, the maximum β value agrees well with recently published values for Gd, Tb, and Ho.[26] The variation in the absorptive part, β, corresponds to a variation in the average absorption length, and thus to a information depth along the surface normal that varies between 240 Å at 1305 eV and 17 Å in the resonance maximum at 1292 eV (calculated for an angle of incidence of $\Theta = 8.7°$ with respect to the surface); since the magnetic scattering cross section is strongly enhanced at energies where the probing volume is small,[26] we observe a strong magnetic signal for a wide range of photon energy. This gives us the opportunity to choose the probing depth without loosing the strong signal. We shall now make use of these resonance properties to determine the depth-resolved magnetic structure.

C. Depth profiles

In order to study the magnetic structure during the FM to AFM phase transition in a depth-resolved way, we performed temperature-dependent reflectivity measurements at various photon energies around the Dy M_5 absorption edge. In Fig. 7, reflectivity scans from a 180-ML-thick Dy film are shown, taken at 1305 eV (upper panels), and 1293 eV photon energy (lower panels) at two different temperatures. In all panels the scans taken during cooling down are compared to those taken at the same temperature on the warming-up path. The superstructure-peak intensities are temperature dependent for mainly two reasons: first, because of the temperature dependence of the magnetic order parameter and second because the thickness of that part of the film that does exhibit helical order grows as well. The latter is the effect we are interested in. Since on the full cooling path the film is helically ordered

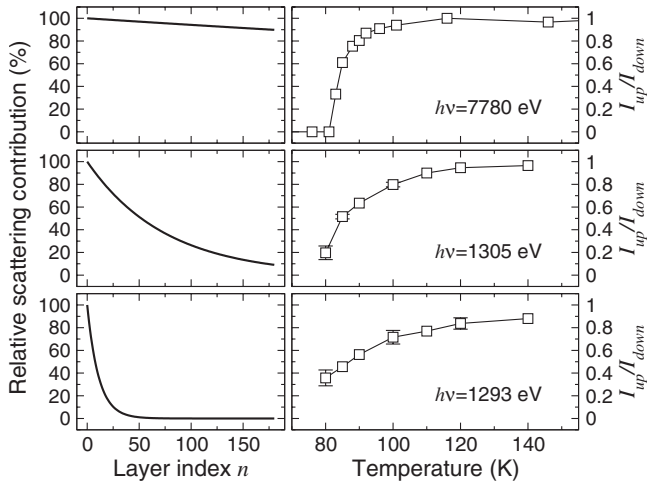

FIG. 8. Left: relative contribution to the scattered intensity as a function of layer index n. The data were calculated for the different photon energies and for the respective scattering angle using the β values from Fig. 6. While in the conventional x-ray region all layers contribute essentially with the same strength to the scattered intensity, only intensity from the topmost layers can be detected near the M_5 resonance at 1293 eV. Right: ratio of intensities measured on the warming and cooling path, I_{up}/I_{down}, for the respective photon energies.

over its full thickness, as can be seen from the value of $W_{q,\perp}$ in Fig. 3(c), the ratio of intensities taken during warming up (I_{up}) and intensities taken on the cooling path (I_{down}) contains the information on the number of antiferromagnetically ordered layers *in the probed volume*—the temperature-dependent ordering parameter is eliminated in this ratio as well as effects due to the change in the observation angle since the satellite position is the same on the cooling and warming paths, as can be seen in Fig. 3(d).

The right panel of Fig. 8 displays the ratio I_{up}/I_{down} for different photon energies. Due to the weak absorption at 7780 eV photon energy (top row in Fig. 8), the contribution to the scattering signal (shown in the left panels of Fig. 8) is nearly the same for all layers of the film. Since the integrated satellite intensity is proportional to the number of contributing layers, I_{up}/I_{down} for this photon energy reflects the number of antiferromagnetically ordered layers normalized to the total number of layers. On the other hand, when strong absorption limits the probed sample volume to a region near the surface, the measured intensity contains information on the number of antiferromagnetically ordered layers in this part of the film. The whole data set hence contains information on the magnetic depth profile.

For temperatures just above the phase transition temperature, the relative peak intensity changes immediately for all photon energies, also in the most surface sensitive scans. From this one can already conclude that the helical phase starts to grow near the surface.

For a quantitative analysis we simulated the scans according to Eq. (1) and integrated the simulated spectra in the same way as the experimental data. The β values determined from the same film allow the analysis of the scattering amplitude of each individual layer n at depth d_n, which is essentially reduced by $e^{-\mu d_n/\sin\theta}$; here $\mu=4\pi\beta/\lambda$ is the absorption coefficient. $W_{q,\perp}$ is a smooth function of the temperature on the heating path and the high-temperature value of $W_{q,\perp}$ corresponds to a single AFM phase along the film normal. We hence can exclude a model, where several helical regions nucleate at different depths in the film. Such a model with several nucleation centers would lead to a discontinuity of

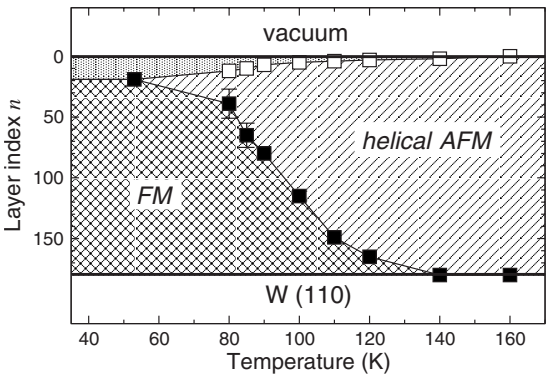

FIG. 9. Magnetic depth profile of a 180-ML-thick Dy film during the transition from the FM to the helical-AFM phase. The data for temperatures $\geq$80 K were calculated from the intensity ratios shown in the right panels of Fig. 8. The helical-AFM phase develops essentially from the Dy surface to the Dy/W interface upon heating. In the near-surface area, there is a different AFM structure (gray shaded region) with a larger period length that persists into the FM phase. Its thickness at 50 K in determined from an analysis of the background as in Fig. 10.

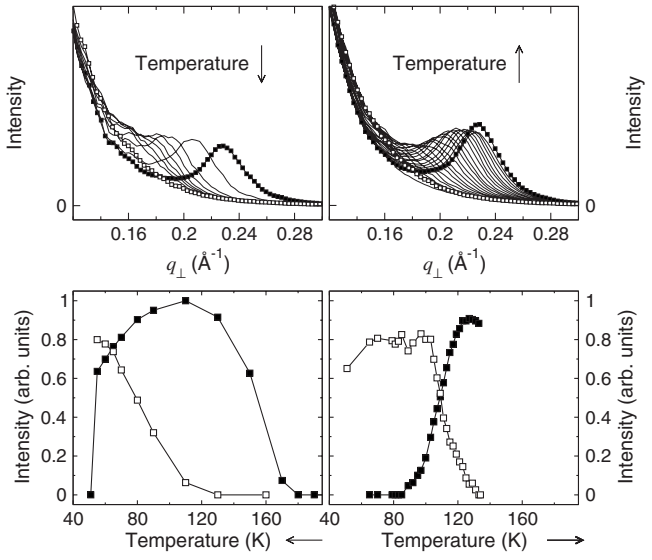

FIG. 10. Detailed view on the change in the magnetic structure in the near-surface region during the phase transition. The data were recorded from an 144 ML Dy film grown on W(110). Left upper panel: spectra during cooling down. Right upper panel: spectra recorded on the warming-up path as indicated by the arrows. A smooth transition between two different helical magnetic structures is visible. The corresponding lower panels display the peak heights of the main satellite (filled symbols) and the changes in the background representing the deviation of the helical structure in the near-surface region (open symbols).

$W_{q,\perp}$ at the temperature, where the separated helical regions merge, which is not observed in the data. Accordingly we simulate the intensity scattered from the film that is only partially helically ordered with a helix that starts in layer n_1 and ends in layer n_2. The ratio I_{up}/I_{down} can be calculated when we use $n_1=1$ and $n_2=N$ for I_{down} from the fully antiferromagnetically ordered film. At resonance maximum, the observed intensity does not depend much on n_2, and n_1 can be calculated. By using this value for n_1 to calculate the 1305 eV data, one finally obtains n_2, and thus the magnetic depth profile presented in Fig. 9. It reveals that the AFM phase grows essentially from the surface toward the substrate over a temperature interval of about 50 K. This means that the FM phase is stabilized at the interface, probably because of uniaxial strain induced by the substrate as mentioned above.

Interestingly, the helical magnetic structure does not develop simply from one boundary to the other but starts in the near-surface region and develops gradually in both directions. Thus, during the phase transition, the magnetic structure consists of three different regions. In the topmost region, the magnetic structure deviates from FM alignment, even at low temperatures in the FM phase. This region can be described as a helical-magnetic phase with a larger period length (gray shaded area in Fig. 9). Because the region is very thin, the diffraction signal is rather broad and only visible from the shape of the background intensity as measured close to the resonance maximum, where the experiment is more surface sensitive. This is illustrated in Fig. 10. The scans were taken at a photon energy of 1294.8 eV, where the signal is sensitive to an extended surface region of about 60 Å, and show how the main peak evolves into a broad component during cooling down (left upper panel) and recovers when heated up (right upper panel). The change in the background between $q_\perp=0.13$ and 0.17 $Å^{-1}$ (open symbols), a measure of the surface helical phase as compared to the peak height of the main satellite (filled symbols), is shown in the respective lower panels. In both directions, there is a smooth transition from one to the other component in the near-surface region. Thus, the remaining helical phase at the surface is the starting point or the seed layer of the developing helical-AFM structure.

V. CONCLUSIONS

To investigate the magnetization profile at the transition between the FM and the helical-AFM phase in Dy-metal films grown on W(110), we made use of the dramatic changes in the photon mean-free path in the region of the Dy M_V absorption threshold. Unlike the systems with two equal boundaries studied so far, this transition is non abrupt in Dy/W(110). We could show that the helical structure grows gradually over a temperature interval of about 50 K starting from a seed layer at the sample surface region to the Dy/W interface. The magnetic structure of the surface region reveals a small modulation even in the fully FM state. Such modifications of the magnetic structure near surfaces should be taken into account when surface sensitive methods are applied.

ACKNOWLEDGMENTS

Expert support by the staff members of BESSY and the ESRF is gratefully acknowledged, particularly the commitment of G. Grübel. The work was financially supported by the BMBF, Projects No. 05KS1KEE/8 and No. 03ZA6BC2, as well as the SFB-290 (TPA06) of the DFG.

*Corresponding author. Present address: Shell International Exploration & Production, Kesslerpark 1, 2288 GS, Rijswijk, The Netherlands; holger.ott@shell.com

[1] W. Nolting, T. Dambeck, and G. Borstel, Z. Phys. B: Condens. Matter **90**, 413 (1993).
[2] W. Nolting, T. Dambeck, and G. Borstel, Z. Phys. B: Condens. Matter **94**, 409 (1994).
[3] M. Bode, M. Getzlaff, and R. Wiesendanger, Phys. Rev. Lett. **81**, 4256 (1998).
[4] M. Bode, M. Getzlaff, A. Kubetzka, R. Pascal, O. Pietzsch, and R. Wiesendanger, Phys. Rev. Lett. **83**, 3017 (1999).
[5] D. Wegner, A. Bauer, A. Rehbein, and G. Kaindl, Jpn. J. Appl. Phys. **45**, 1941 (2006).
[6] D. Wegner, A. Bauer, and G. Kaindl, Phys. Rev. B **73**, 165415 (2006).
[7] C. Schüßler-Langeheine, R. Meier, H. Ott, Z. Hu, C. Mazumdar, A. Yu. Grigoriev, G. Kaindl, and E. Weschke, Phys. Rev. B **60**, 3449 (1999).
[8] C. Schüßler-Langeheine, H. Ott, A. Yu. Grigoriev, A. Möller, R. Meier, Z. Hu, C. Mazumdar, G. Kaindl, and E. Weschke, Phys. Rev. B **65**, 214410 (2002).
[9] B. Kim, A. B. Andrews, J. L. Erskine, K. J. Kim, and B. N. Harmon, Phys. Rev. Lett. **68**, 1931 (1992).
[10] G. A. Mulhollan, K. Garrison, and J. L. Erskine, Phys. Rev. Lett. **69**, 3240 (1992).
[11] C. Schüßler-Langeheine, E. Weschke, C. Mazumdar, R. Meier, A. Yu. Grigoriev, G. Kaindl, C. Sutter, D. Abernathy, G. Grübel, and M. Richter, Phys. Rev. Lett. **84**, 5624 (2000).
[12] E. Weschke, H. Ott, E. Schierle, C. Schüßler-Langeheine, D. V. Vyalikh, G. Kaindl, V. Leiner, M. Ay, T. Schmitte, H. Zabel, and P. J. Jensen, Phys. Rev. Lett. **93**, 157204 (2004).
[13] C. Schüßler-Langeheine, E. Weschke, A. Y. Grigoriev, H. Ott, R. Meier, D. V. Vyalikh, C. Mazumdar, C. Sutter, D. Abernathy, G. Grübel, and G. Kaindl, J. Electron Spectrosc. Relat. Phenom. **114-116**, 953 (2001).
[14] J. Jensen and A. R. Macintosh, *Rare Earth Magnetism* (Clarendon Press, Oxford, 1991).
[15] F. J. Darnell, Phys. Rev. **130**, 1825 (1963).
[16] F. Tsui and C. P. Flynn, Phys. Rev. Lett. **71**, 1462 (1993).
[17] M. B. Salamon, S. Sinha, J. J. Rhyne, J. E. Cunningham, R. W. Erwin, J. Borchers, and C. P. Flynn, Phys. Rev. Lett. **56**, 259 (1986).
[18] R. S. Beach, J. A. Borchers, A. Matheny, R. W. Erwin, M. B. Salamon, B. Everitt, K. Pettit, J. J. Rhyne, and C. P. Flynn, Phys. Rev. Lett. **70**, 3502 (1993).

[19] H. Ott, C. Schüßler-Langeheine, E. Schierle, G. Kaindl, and E. Weschke, Appl. Phys. Lett. **88**, 212507 (2006).
[20] D. Gibbs, M. Blume, D. R. Harschman, and D. B. McWahn, Rev. Sci. Instrum. **60**, 1655 (1989).
[21] G. Helgesen, J. P. Hill, T. R. Thurston, and D. Gibbs, Phys. Rev. B **52**, 9446 (1995).
[22] B. L. Henke, E. M. Gullikson, and J. C. Davis, At. Data Nucl. Data Tables **54**, 181 (1993).
[23] C. T. Chantler, K. Olsen, R. A. Dragoset, A. R. Kishore, S. A. Kotochigova, and D. S. Zucker, 2005, http://physics.nist.gov/ffast
[24] L. G. Parratt, Phys. Rev. **95**, 359 (1954).
[25] M. Blume and D. Gibbs, Phys. Rev. B **37**, 1779 (1988).
[26] H. Ott, C. Schüßler-Langeheine, E. Schierle, A. Yu. Grigoriev, V. Leiner, H. Zabel, G. Kaindl, and E. Weschke, Phys. Rev. B **74**, 094412 (2006).